

CAAP Annual Report

Date of Report: *October 7, 2020*

Contract Number: *693JK31850009CAAP*

Prepared for: *U.S. DOT Pipeline and Hazardous Materials Safety Administration*

Project Title: *New Bio-Inspired 3D Printing Functionalized Lattice Composites for Actively Preventing and Mitigating Internal Corrosion*

Prepared by: *North Dakota State University*

Contact Information: *Mr. Andrew Mahoney, M.S. student, Email: Andrew.mahoney@ndsu.edu; Mr. Matthew Pearson, M.S. student, Email: matthew.pearson@ndsu.edu, Phone: 701-231-7204; Dr. Hong Pan, Postdoc, Email: hong.pan@ndsu.edu; Mr. Adeeb Ibne Alam, PhD student, Email: adeeb.alam@maine.edu; Dr. Zhibin Lin, Email: zhibin.lin@ndsu.edu, Phone: 717-231-7204; Dr. Bashir Khoda, Email: bashir.khoda@ndsu.edu, Phone: 701-231-7195*

For quarterly period ending: *October 7, 2020*

Business and Activity Section

(a) Generated Commitments

No-cost extension will be made to the existing agreement

Purchase made for the nano-materials, and the 3-D printable polymers

(b) Status Update of Past Quarter Activities

The research activities in the 2nd annual report included: (i) Task 2: Completed complementary efforts on tensile behavior of the 3D printing lattice structures; (ii) Task 5: Completed efforts on characterization of functional materials; (iii) Task 6: Developed the Implementation Plan II with a new

design of integrating 3D printing composites with robot tools for field application. Durability tests of the new 3D printing lattice composites are in progress.

(c) Cost share activity

Cost share was from the graduate students' tuition waiver.

(d) Summary of detailed work for Tasks 2, 5, and 6

Task 2: Fabricate, Characterize and Optimize 3D printing lattice composites

A comprehensive and systematic study of new 3D printing lattice composites was conducted for characterizing their mechanical and chemical properties.

Among them, we missed the tensile property of the lattice structures. We reported our early attempt on early document on the tensile test by mounting metal sheet at back of the samples, but most samples failed by locally interfacial bond, which did not help to generate accurate tensile property of the lattice. Thus, another attempt was made to perform the direct tensile test to complement the test matrix in this period.

2.2.1 Tensile properties of 3D printing lattice structures

2.2.1.1 Sample preparation for macro-scale tensile test

This section aimed to understand tensile behavior of the 3D printing lattice members. We used the PLA purchased from Hatchbox to print the specimens. The specimens were drawn in Rhino 6 and using custom VB Scripts first the toolpaths were generated and then the G-codes were generated for each specimen, as shown in **Fig. 1**. For every print, the parameters were kept constant. The bed temperature was 70° C and the nozzle temperature was 205° C for each print. The specimens have an outer dimension of 5.0 mm diameter and 72 mm height. They were printed in a vertical way to have each layer of the filter in horizontal order.



Fig. 1. Generated G-code of the specimens using Rhino6, LS type (Left), R type (right)

2.2.1.2 Test setup

Mechanical properties of 3D printing samples, i.e., tensile strength and tensile behavior in macro scale, was characterized using an Instron 5882 universal testing machine, as shown in **Fig. 2**. The 3D printing samples were selected with pore size of 0.4-, 0.6-, and 0.8-mm for both LS and R types.

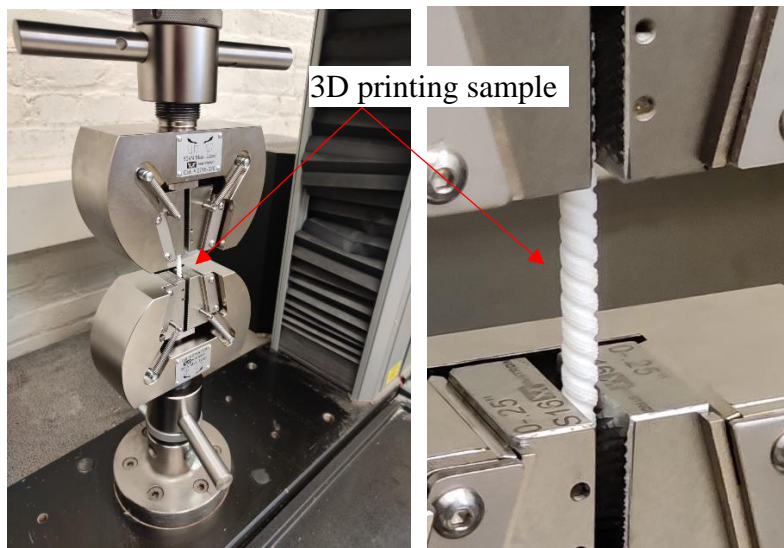
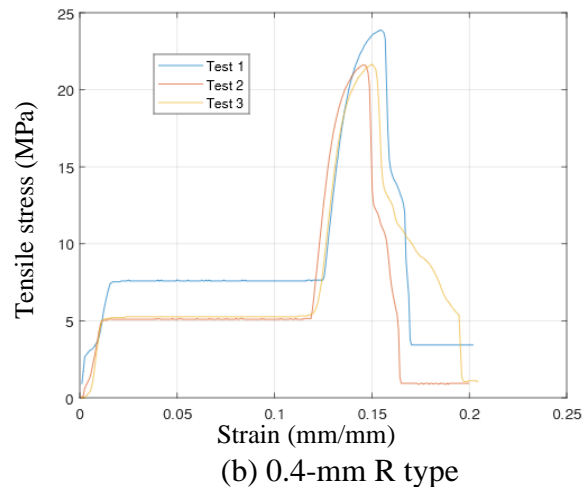
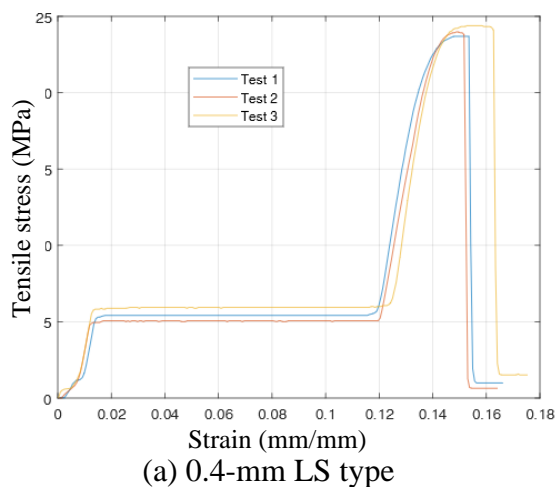


Fig. 2. Test setup

2.2.1.3 Test results and discussion

The tensile property of the 3D printing lattice structures was plotted in **Figs. 3(a)-3(f)**. Similar trend to their compression was observed on tensile stress-strain relation through three stages were observed: (a) pre-yielding; (b) plateau; and (c) post strain-hardening behavior.

As illustrated in **Figs. 3(a)-3(f)**, before yielded, all lattices behaved nearly linear. Clearly, 0.4-mm and 0.6-mm LS/R patterned lattice samples started to yield about 5.0~10.0 MPa. After that, the lattice exhibited a long plateau, and then quickly displayed a strain-hardening/necking behavior due to polymer permanent deformation. However, with the pore size increase, as illustrated in **Figs. 3(e)-3(f)**, 0.8-mm LS/R patterned lattice samples showed different behavior, where LS type samples had no apparent strain-hardening behavior (see **Fig. 3(e)**), and R patterned lattice started strain hardening behavior just after yielding (see **Fig. 3(f)**), without plateau as other cases did.



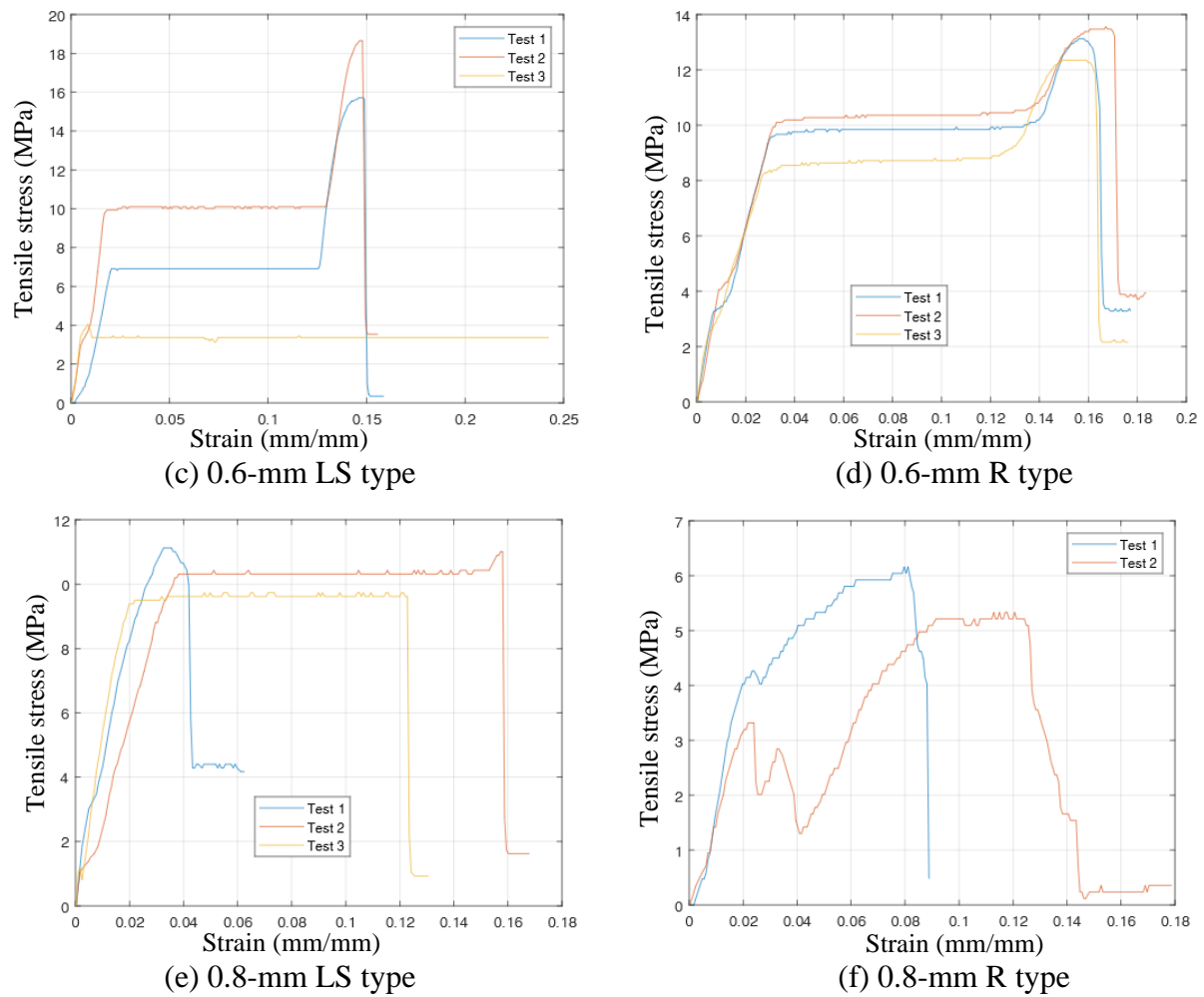


Fig. 3. Tensile stress-strain curve for both LS/R type samples

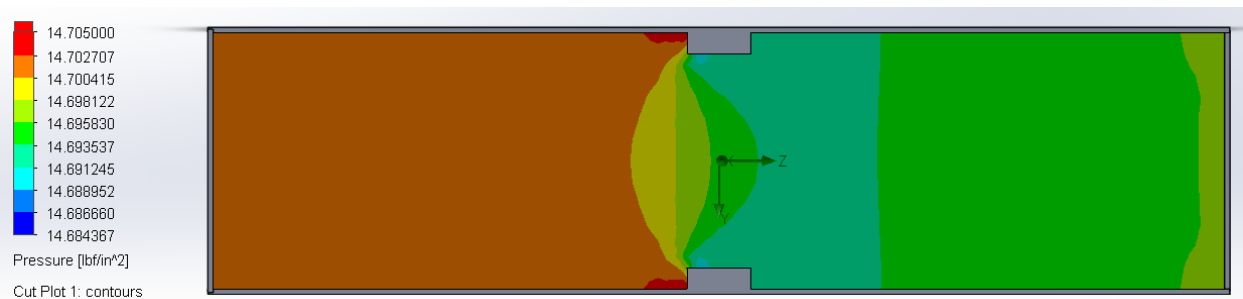
Task 5: Characterize the new composite systems

This task aimed to conduct a comprehensive experimental investigation to characterize the properties of the new 3D printing lattice composite system and particularly the features of characterize and optimize the chemical activities of the new 3-D printing composites

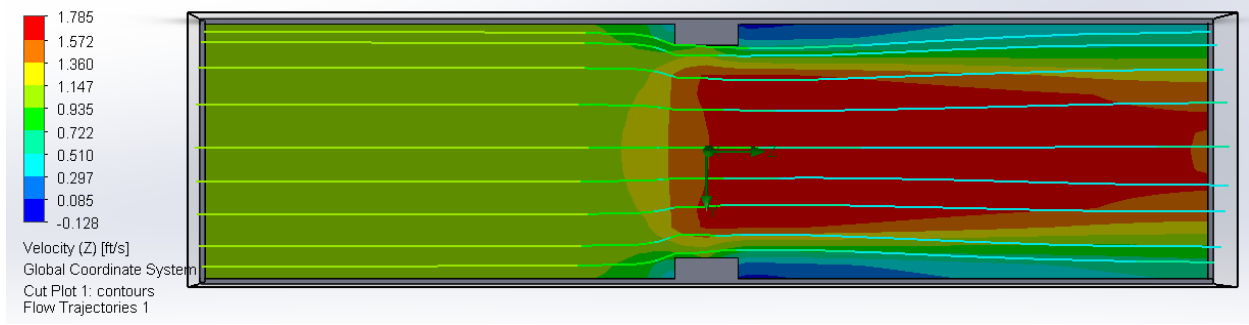
- Numerical simulation to identify and optimize the design parameters

Finite element method (FEM), as a numerical tool, was used to simulate a similar situation with the real state. The three-dimensional (3-D) pipes under different cases were modeled, where mixed water and hexadecane were considered.

As typically illustrated in **Figs. 4a and 4b**, the results of the Finite Element Method were presented and discussed in Section 3.



(a) Pressure contour



(b) Velocity contour

Fig. 4 FE results of the pipe under different cases.

5.1 Continuous efforts on design of 3D printing lattice structures

We developed a customized multi-material delivery system to print the porous structure with lattice architecture within five-micron spatial accuracy. As well known, periodic cellular structure is the most known man-made cellular structure which are used in the design of light weight sandwich panel structures.

5.2 Continuous efforts on composites

We selected the PLA and ABS as our base for printing materials in that there were no preferable 3D printable materials so far.

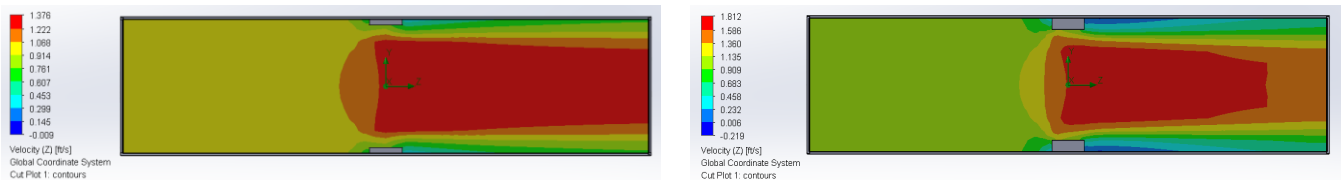
Surface morphologies of pristine samples and modified ones were observed by Scanning Electron Microscopy (SEM, JEOL, Japan) and the elemental distribution of the as-prepared samples were investigated by Energy-dispersive X-ray Spectroscopy (EDS) attached to SEM.

5.3 Results and discussion

5.3.1 Effects of the composite thickness on the flow conditions

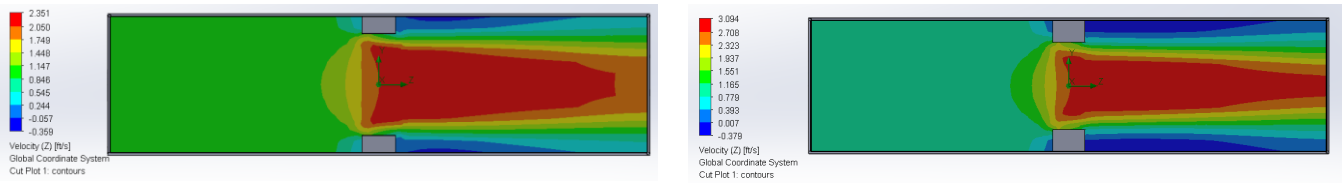
This group of the simulation was to understand the impacts of composite thickness on the flow conditions, and the findings could help to design the composite layers.

Figs. 5 and 6 were plotted in the cross-sectional view in contour, where flow velocity was 1.0 ft/s and initial pressure was about 15 psi, and pipe dimension was 24-in in diameter. Clearly, the flow conditions (velocity or rate in **Fig. 5** and pressure in **Fig. 6**) were disturbed near the location of the composite layers. With the increase of the thickness, the initial flow rate raised up to over 3 times higher at the narrow pathway than those at other locations, particularly when at the composite layer of $T_c = 4.0$ in as expected. Differently, the flow pressure was less disturbed by the composite layers by less 0.2% over all cases, with slightly more uniformly distribution over the whole flow. Note that the fluid viscosity (friction) such as oil type fluid was not considered in this stage, and we will discuss that in the further study.



(a) $T_c = 1.0$ in.

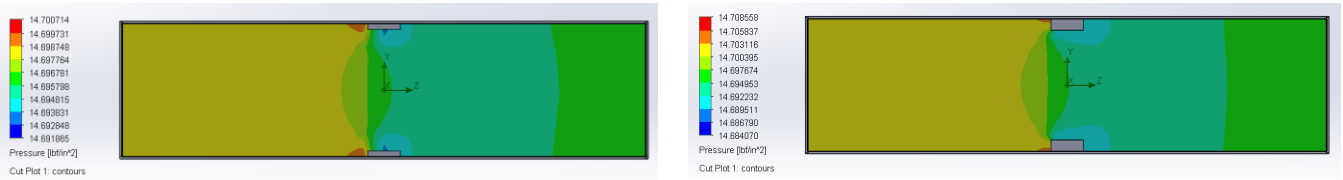
(b) $T_c = 2.0$ in.



(c) $T_c = 3.0$ in.

(d) $T_c = 4.0$ in.

Fig. 5 Impacts of different composite thickness on the flow conditions (velocity) by $D_p=24$ -in dia.



(a) $T_c = 1.0$ in.

(b) $T_c = 2.0$ in.



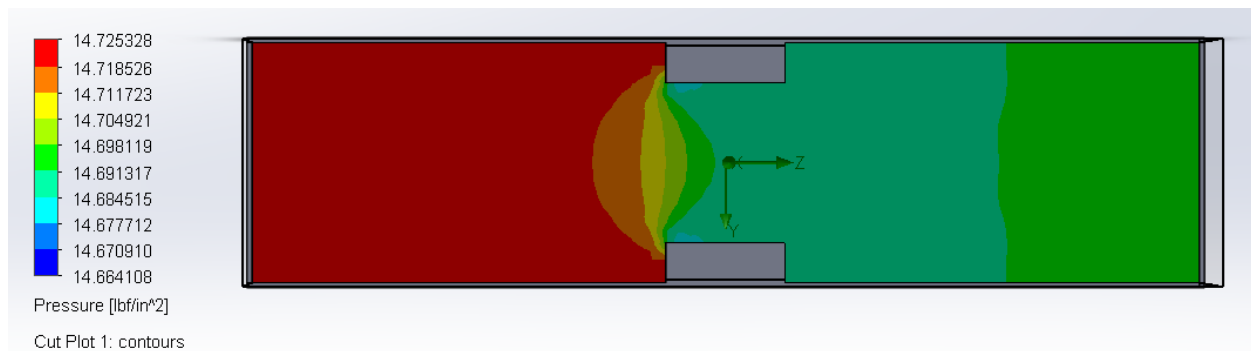
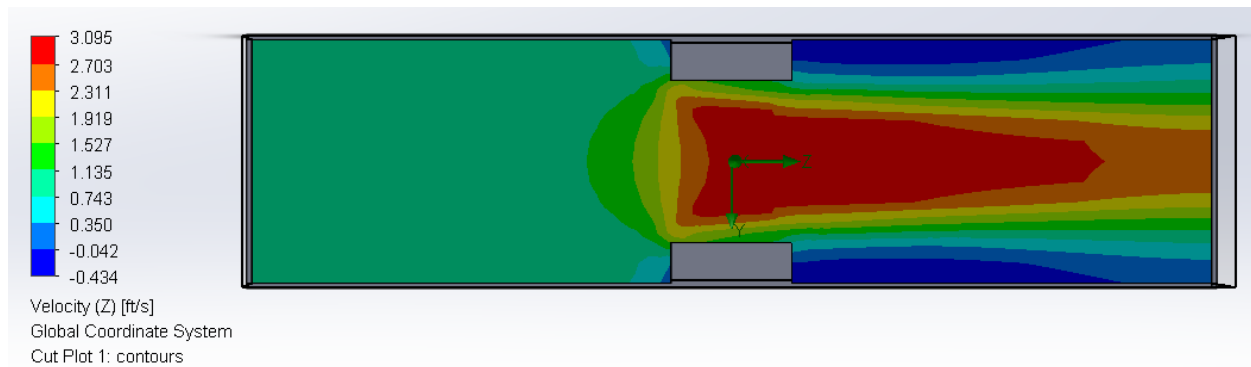
(c) $T_c = 3.0$ in.

(d) $T_c = 4.0$ in.

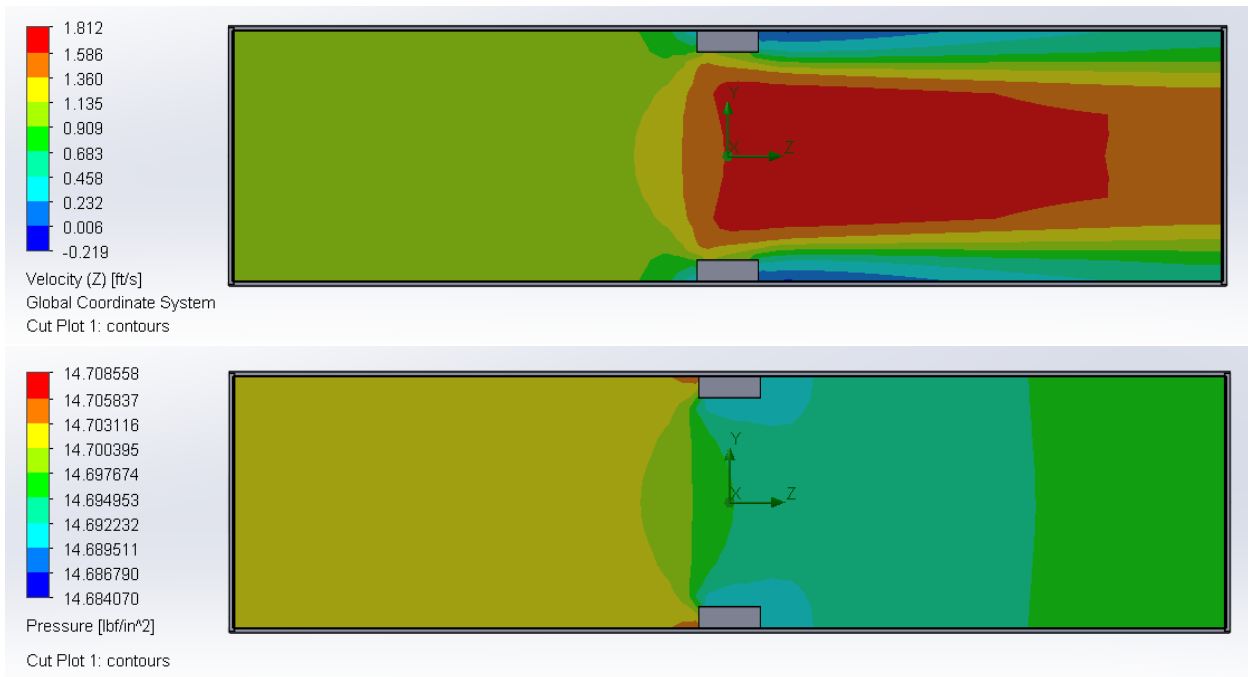
Fig. 6 Impacts of different composite thickness on the flow conditions (pressure) by $D_p=24$ -in dia.

5.3.2 Effects of the diameter size on the composite layers

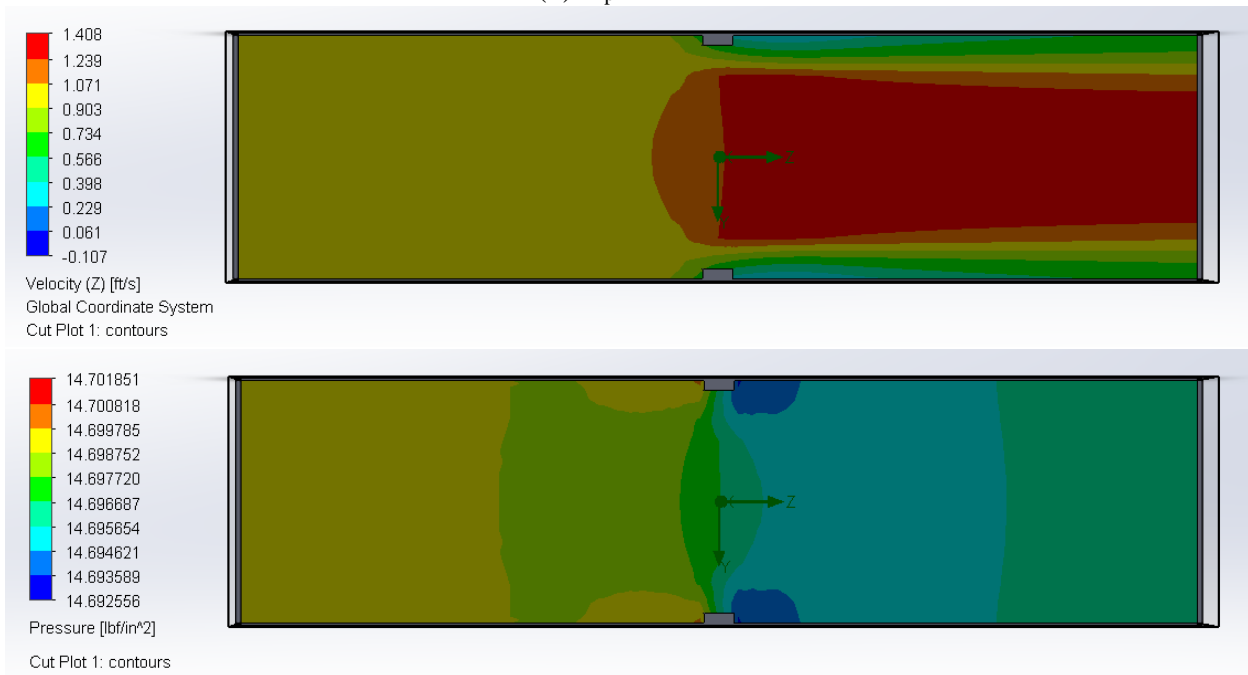
To better qualitatively determine the effectiveness of the composite layers under varying pipe sizes, three typical sizes, 12-, 24-, and 48-in diameters, were selected from small to large scale pipes. The results were shown in **Figs. 7 and 8**, where different diameters and different composite thickness were presented. Clearly, with the increase of the pipe size, the composite layers have less sensitivity to flow conditions (velocity and pressure).



(a) $D_p = 12$ in.

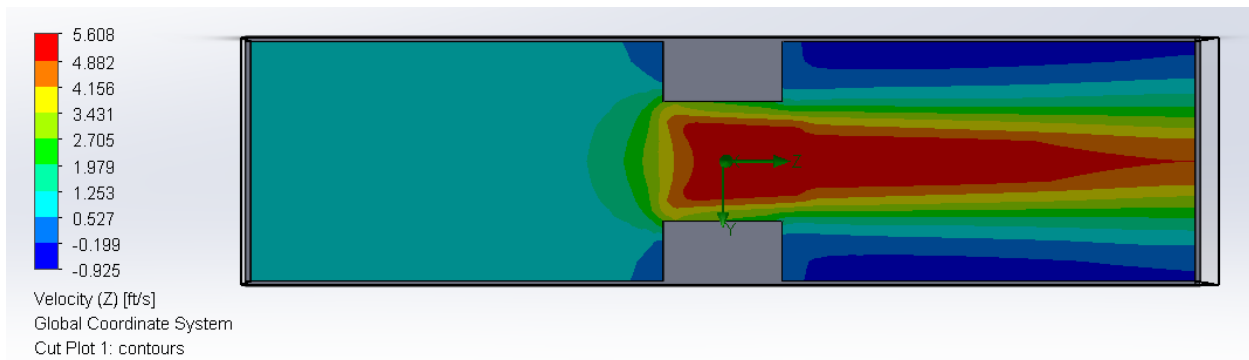


(b) $D_p = 24$ in.

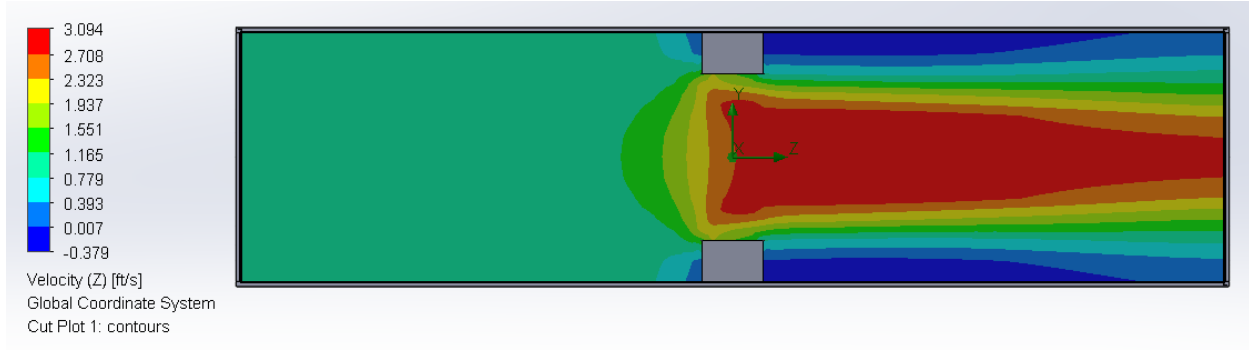


(c) $D_p = 48$ in.

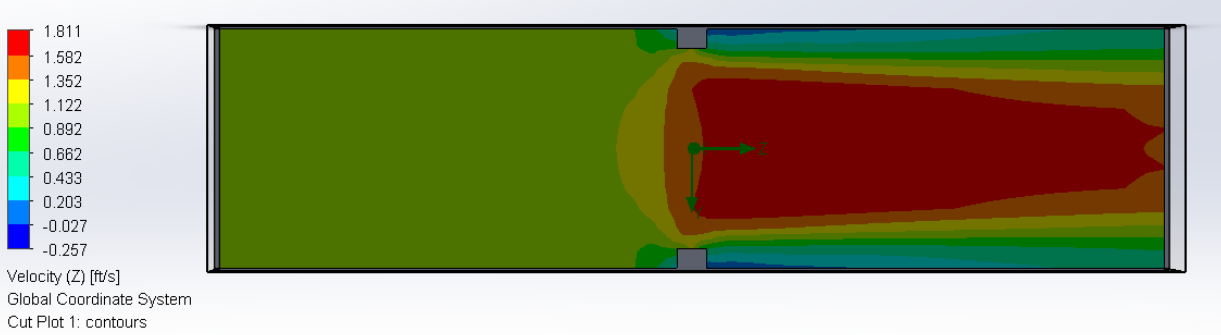
Fig. 7 Impacts of pipe sizes on the composites by $T_c = 2.0$ in.



(a) $D_p = 12$ in.



(b) $D_p = 24$ in.



(c) $D_p = 48$ in.

Fig. 8 Impacts of pipe sizes on the composites by $T_c = 4.0$ in.

5.3.3 Effects of the initial flow velocity on the performance of the composite layers

Consider that actual gas pipe could use the initial velocity reach up to 30~60 ft/s, the initial flow velocity could affect the performance of the composite layers on the internal surface of a pipe. The results were shown in **Fig. 9**. The major trend in the flow conditions (velocity and pressure) was identical. The resulting flow velocity was approximately proportional to the amplitude of the initial flow rate, while the resulting flow pressure, illustrated in **Fig. 10**, raised with the increase of the flow velocity as expected.

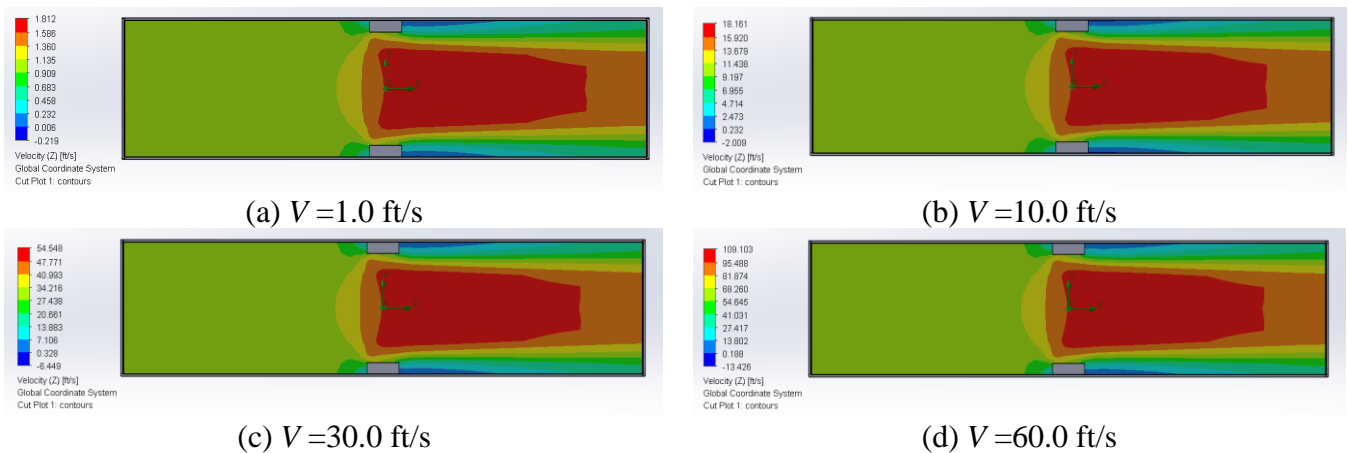
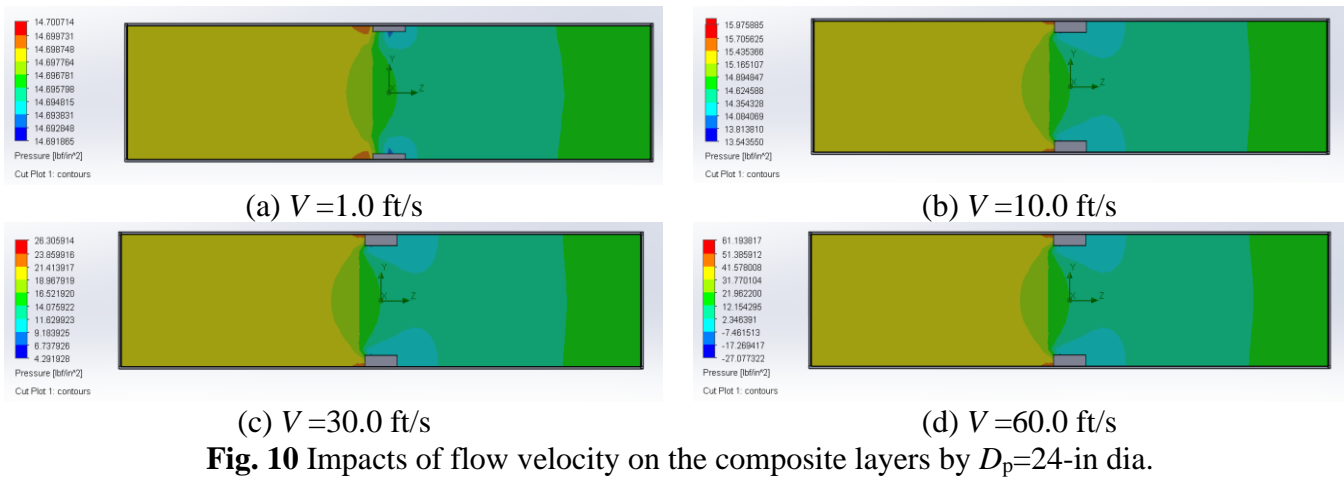


Fig. 9 Impacts of flow velocity on the composite layers by $D_p = 24$ -in dia.



Task 6: Assess long-term durability tests of the new composite systems

6.1 Pump system.

As we discussed at last report, the attempts were made to increase the applications of the designed lattice structures for accommodating pipe environment. This study will continue this effort to provide a concept design using a pump system and elucidate the critical design parameters for Task 8.

The initial test set up was assembled in detail for calibrating the design concept. The syringe pump machine was from the standardized KD Scientific. The machine allows for a variable and/or constant infuse/withdraw flow rate and force rate to provide for precise flow volume moved throughout the attached flow system, as typically shown in **Fig. 11**.



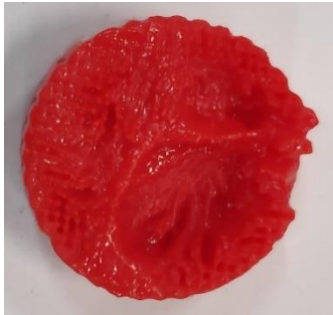
Fig. 11 Snapshot of extraction process of water

6.2 Surface modification from 3D printing.

(a) PMMA coat of PLA: Poly Methyl Methacrylate (PMMA) has a good binding property and inert in nature. It is tough and has high melting temperature (~ 220 C). To protect the filter, we dipped the filters in a Polymethyl methacrylate (PMMA) and 1,3- Dioxolane solution to get a layer of PMMA over the PLA structure. PMMA is much more inert than PLA, which potentially could survive the surface treatment. Dioxolane is the solute in this solution, which was supposed to be evaporated quickly to get a PMMA layer over PLA. Unfortunately, the filters could not survive after dipping into the solution. They became soft and mushy as shown below.

20%(w/w), 10%(w/w) PMMA-dioxolane solution and only dioxolane were used to check the feasibility, as shown in **Fig. 12**. PLA happens to react with dioxolane, dioxolane works as a welding agent for the PLA. To explain, the pores of the structure are very small, which increases the total surface area. As dioxolane gets entrapped into the pores, it does not evaporate that fast. Dioxolane also gets

enough time to react with the PLA, with a high surface contact. Due to that some of the pores get blocked and the structure becomes soft.



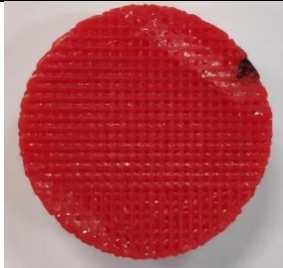
(a) 10%(w/w) PMMA-dioxolane solution



(b) Only dioxolane

Fig. 12 3D printing PLA lattice dipped in PMMA-dioxolane solution.

(b) Epoxy coating of PLA: We also tried to make layer of epoxy over the PLA by dipping the filters into epoxy, as shown in **Fig. 13**. Epoxy resin cat no. ep-3000-32 was used with 1-part hardener and 5-part epoxy resin. The epoxy resin does not react with PLA. But the solution is very viscous, which makes it hard to penetrate the structure with fine pores. First, we tested with larger pores with 1mm LS and 2mm LS filters. If we just dip the filters and use the gravity to drip out the solution, the pores at the lower level gets clogged and the epoxy sets there completely blocking the pores. If we clean the pores with high pressure air before the epoxy sets, it is possible to have some pores to be clear. But for a finely porous structure, it is impossible to say if the pores are blocked or not, even after cleaning with high pressure air.

Type	Original size	Zoomed (4x)
1 mm LS dipped in epoxy resin (fully blocked)		
2 mm LS dipped in epoxy resin (fully blocked)		
1 mm LS dipped in epoxy resin, Pores cleaned with high pressure air (Partially blocked)		

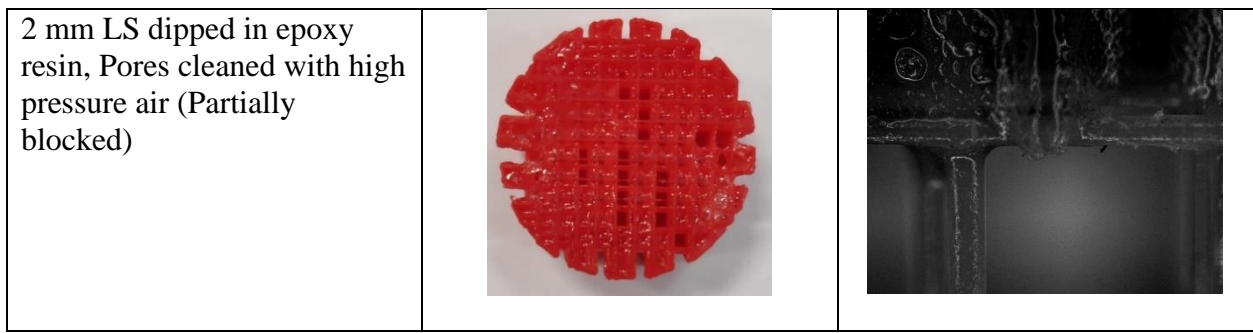


Fig. 13 3D printing PLA lattice dipped in epoxy resin.

(c) Controlling the rheology of epoxy: To lower the viscosity we used acetone, which also has a drastic effect on PLA. The structure gets soft, weak, and discolored after dipping into the epoxy-acetone solution as shown in **Fig. 14**. Further research to be done to get an epoxy resin with low viscosity which does not react with PLA. In this way we can get a PLA filter with a layer of epoxy over the surface of PLA for better long-term durability.

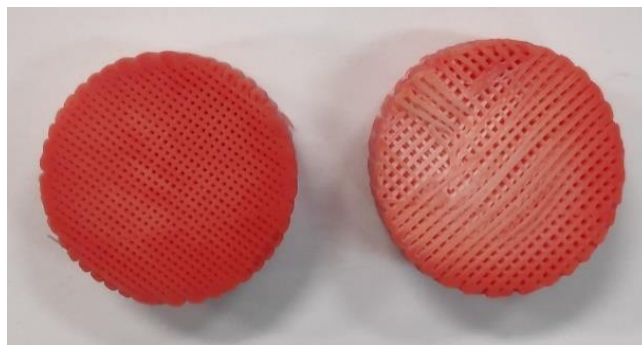


Fig. 14 3D printing PLA lattice dipped in epoxy resin dissolved with acetone.

(e) Description of any Problems/Challenges

No problems are experienced during this report period

(f) Planned Activities for the Next Quarter

The planned activities for next quarter are listed below:

- Continued efforts in Task 6 will be made, including enhanced durability study through multilayer surface treatments, and a different coating application, such as spray coating.
- More efforts on investigation of degradation associated with pressure, including design and characterization of pump-induced pressure and its impacts on the designed composite systems.
- New efforts on the 3D printing ring sample design and optimization.